Chapter 5

Fluctuations and Related Phenomena

In Chapter 3, the effects of stochastic, internal motions are minimized because the parametrically-pumped electron oscillators are resonantly cooled by a standing wave mode of the cavity. Important observed features of coherent motions could be understood using an ordinary differential equation for rigid axial motion of N electrons, a limit which is approached by cooling the internal motions to their zero-point energy. In Chapter 4, however, we observed that the parametric resonance was modified as the electron cyclotron motion was detuned from resonance with a cavity mode. The extraordinary sensitivity of non-rigid, synchronized motions to radiative cooling proved to be a very useful tool for probing standing wave modes in a cavity. A rigid model can not explain the Lorentzian lineshapes of observed cavity mode resonances or even why the parametric axial resonance is at all sensitive to cyclotron damping. Even when cavity cooling of internal motions is maximized, there are interesting non-rigid behaviors in synchronized motions of electron oscillators. We now explore the ways that parametrically-pumped electron oscillators are only partially synchronized above threshold, with observable fluctuations in both amplitude and phase due to internal motions.

Near threshold ($h \approx h_T$, $\omega_d = 2\omega_z$), the character of the quiescent state changes rather dramatically with small change in the pump strength. Fluctuations in the CM motion grow as the pump strength increase toward the threshold, as

shown on magnified scale in Fig. 5.1a, but the coherence time remains short. To observe fluctuations in the signal directly, a storage scope captures the IF signal, externally triggered by a precision frequency synthesizer at the same frequency. Fluctuations persist above the threshold in the synchronized CM motion, with

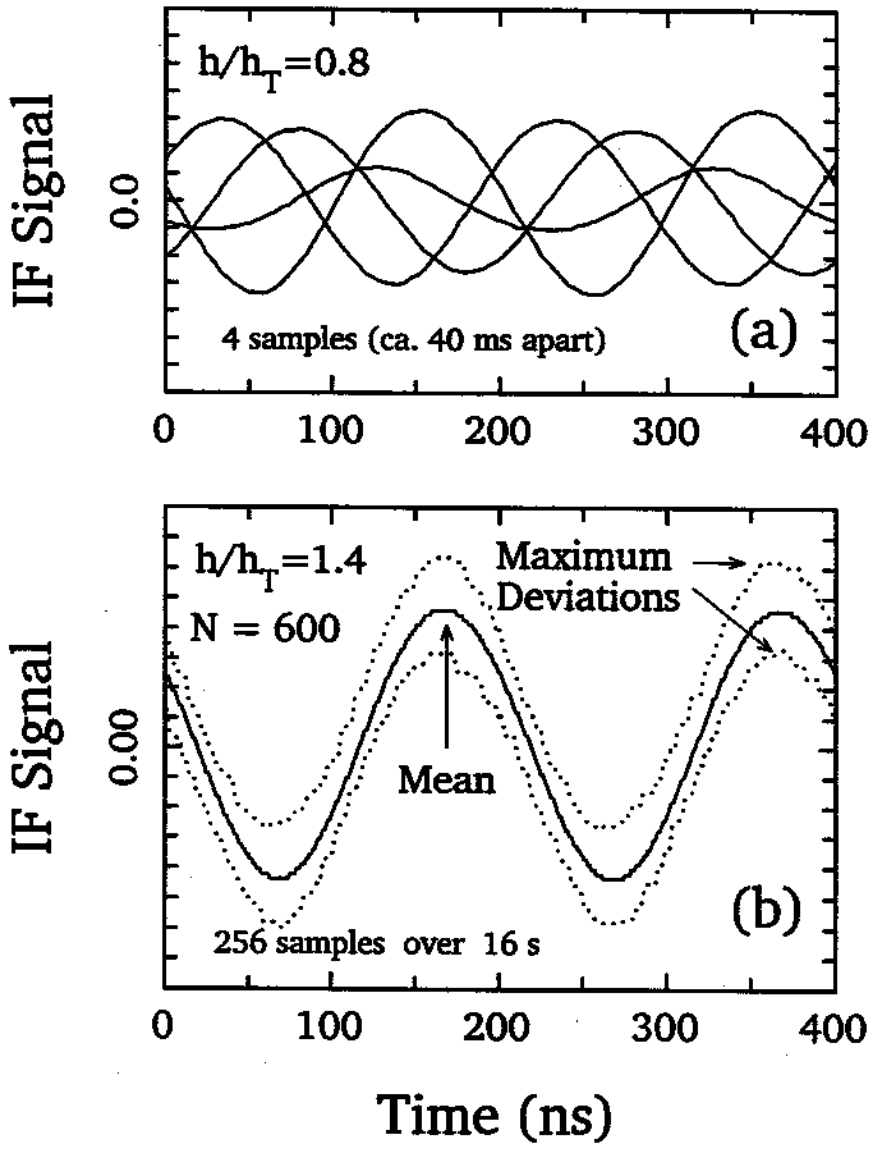

Figure 5.1: Sampled IF signal (5 MHz) illustrates (a) incoherent response for $h < h_T$ and (b) long-term coherence for $h > h_T$. Dotted lines in (b) show maximum deviations from mean coherent motion.

observable deviations (dotted lines in Fig. 5.1b) from a mean coherent oscillation (solid line in Fig. 5.1b) and interesting consequences for this phase bistable system.

5.1 Transitions between Phase Bistable States

Since the system (Fig. 2.17) is invariant under a time translation of one pump period ν_d^{-1}, any coherent response at half the pump frequency must be phase

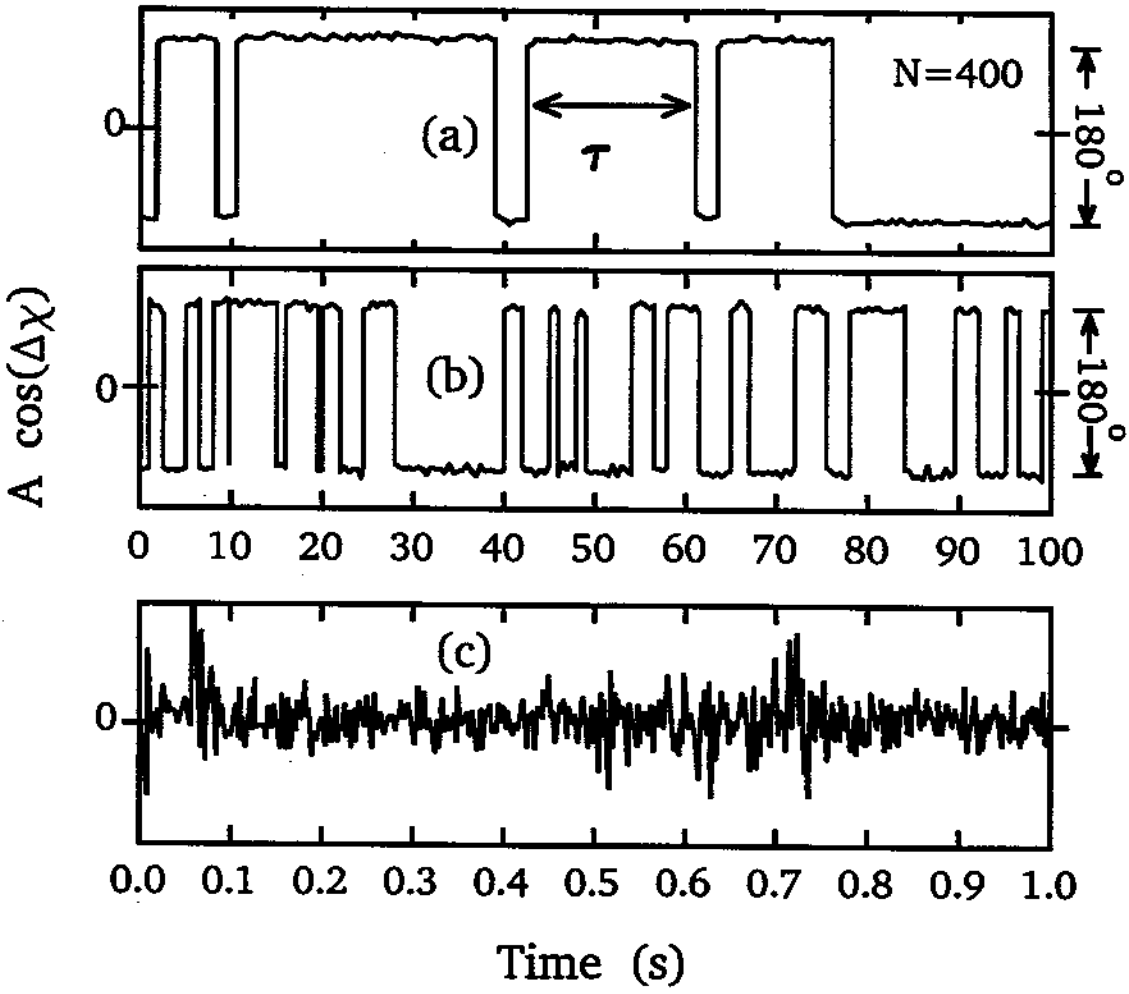

Figure 5.2: Random transitions between phase-bistable states (a)-(b) . Disordered motions (c) result if cyclotron cooling is weak. Residence time τ, illustrated in (a), on average becomes shorter (b) with increasing detuning between cyclotron and cavity mode frequencies.

bistable, with equal likelihood of having either of two steady-state phases which differ by 180°. Fluctuations cause random transitions between these phase states, reminiscent of a two-level system coupled to a heat bath or brownian motion of a particle in a double-well potential. We observe abrupt transitions between the two phases, as illustrated in Fig. 5.2a & b (similar to those attributed to collisions in a much poorer vacuum in an early experiment with only one electron [92]). The time between two consecutive transitions, or the residence time in one phase state, is denoted by τ (Fig. 5.2a). Thousands of flips observed over many hours show the flips to be random with typical distribution of the residence times τ (times between flips) shown in Fig. 5.3a for N = 750 electrons. The distribution fits well to an exponential form (Fig. 5.3b) and is consistent with a two-level model with constant transition probability, except for the shortest times. The first 50-second time bin receives 30 percent of counts from flips occurring within 5 seconds apart. This "over-abundance" of short residence times may be a clue to the mechanism activating the phase-flipping transitions, which is not understood yet.

In more detail, a phase sensitive detector is employed to distinguish between the phase-bistable states. As illustrated in Fig. 2.17, the voltage induced by the synchronized motion across the resistor in the simplified diagram is mixed with a local oscillator at $\nu_d/2$ and the phase of the local oscillator ϕ is adjusted so that the filtered output (near DC) is proportional to

$$A \cos(\Delta\chi) \quad . \tag{5.1}$$

Fluctuations in amplitude A and phase χ of the coherent response (Fig. 5.1) can be observed with a fast storage oscilloscope (after the signal is mixed down to a conveniently lower frequency). The phase fluctuation relative to one phase state χ_{ss} is denoted by

$$\Delta\chi = \chi(t) - \chi_{ss} \quad . \tag{5.2}$$

A transition of the synchronized motion from one phase state to the other ($\chi_{ss} \longrightarrow$

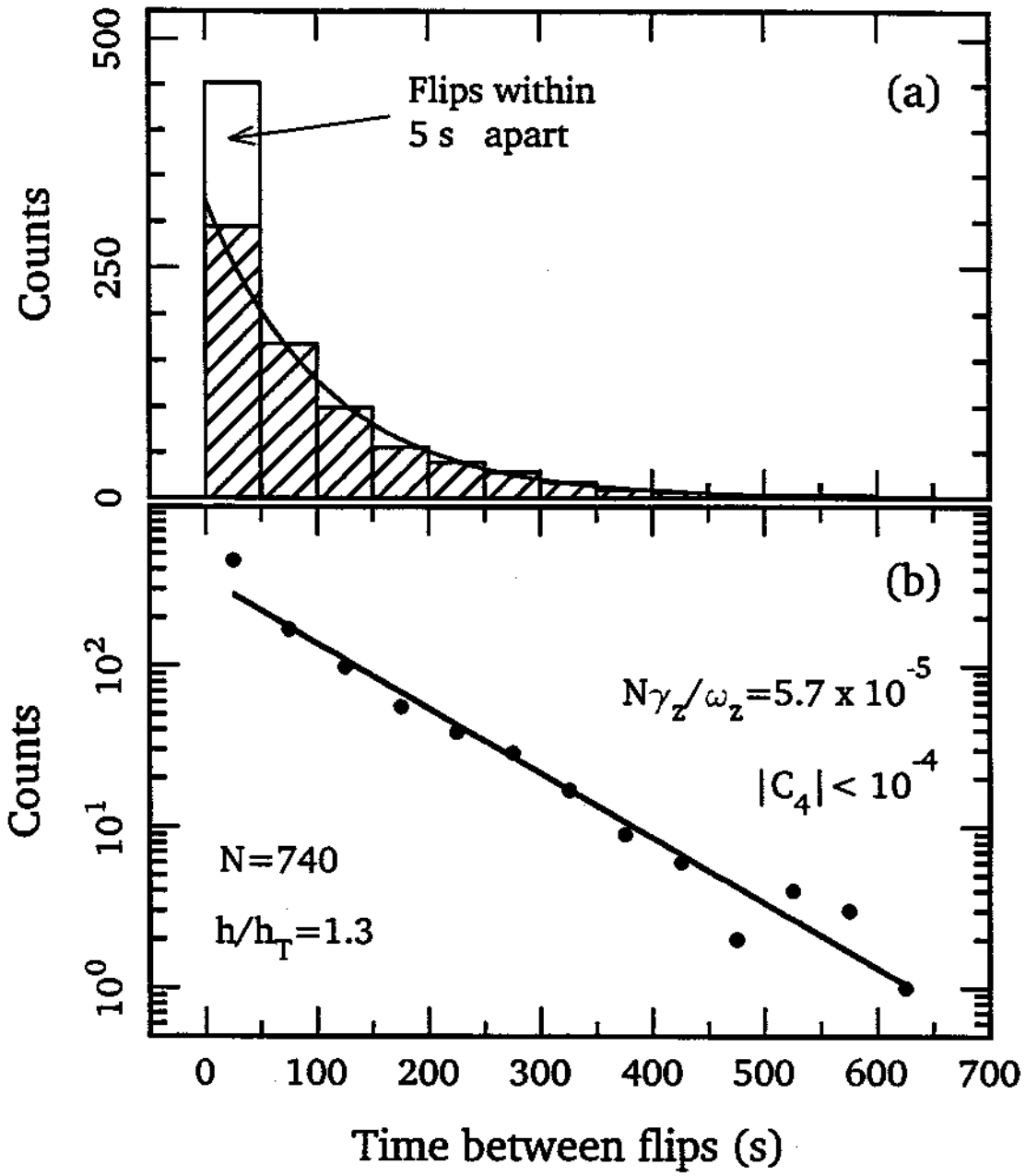

Figure 5.3: (a) Distribution of residence times, and (b) good fit to an exponential form.

$\chi_{ss} + \pi$) is observed as a change in sign of the detected signal

$$A\ \cos(\Delta\chi + \pi) = -A\ \cos(\Delta\chi)\ . \tag{5.3}$$

This signal is related to the projection of the CM "state vector" onto the x-axis in Fig. 3.8 (adjustment of the phase of the local oscillator corresponds to rotating the coordinate system so that the x-axis passes through the steady-states when $\Delta\chi = 0$).

To examine the abrupt transitions from one phase state to the other in great detail, a digital storage oscilloscope is armed to capture the signal when a phase jump occurs. Magnified time resolution on a digital oscilloscope reveals an interesting diversity of phase jump "trajectories" in the synchronized CM motion. Several samples are shown in Fig. 5.4 for $N = 700$ electrons. We observed that in many cases a transition is initiated with a collapse of the CM motion. This is illustrated in Fig. 5.4a. The CM motion is then re-excited to the other phase-state after a being in the "quiescent" state for a "dead time." This dead time can be as long as 100 ms but tends to decrease with increasing pump strength. In some cases, a transition is preceded by a period of observable increased fluctuations (Fig. 5.4 b). Completion of a phase jump may take many attempts in rapid succession (Fig. 5.4c-e). Fig. 5.4f shows a rare event in which the CM motion appears to be oscillating in the "basin" (Fig. 3.8) of one phase-state, switching over to (and then returning from) the other basin with unabated oscillation. (Fig. 5.4a-f were sampled under the same control parameters.) The duration of a phase jump τ_J (defined in Fig. 5.4a), is observed to be roughly in the range 10-100 ms with distributions that depend upon pump strength, anharmonicity and number of electrons (Fig.5.5).

The mean residence time $\bar{\tau}$ in a phase state is observed to vary greatly with control parameters. It increases rapidly with the number of electrons since the fluctuating motions of a larger number of electrons average to a smaller sized fluctuation of their CM motion (Fig. 5.6a). For $N > 2500$, no transition is observed over hours when ω_C' is resonant with a cavity mode (such as TE_{115}). Mean

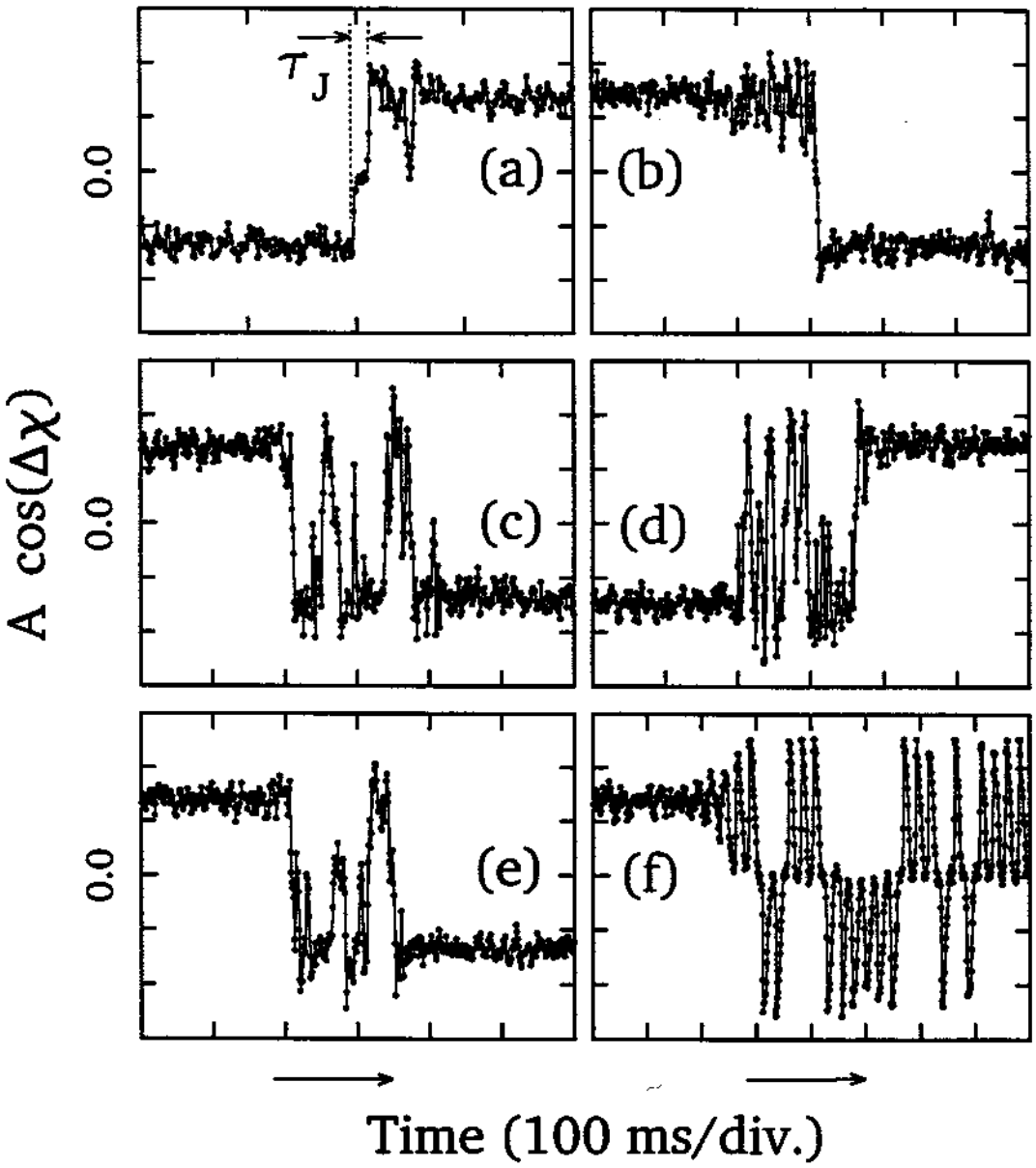

Figure 5.4: Examples of phase jump "trajectories" observed with 600 electrons parametrically driven at $h = 1.4h_T$ ($C_4 \sim -6 \times 10^{-4}$ and $N\gamma_z/\omega_z = 1.2 \times 10^{-5}$).

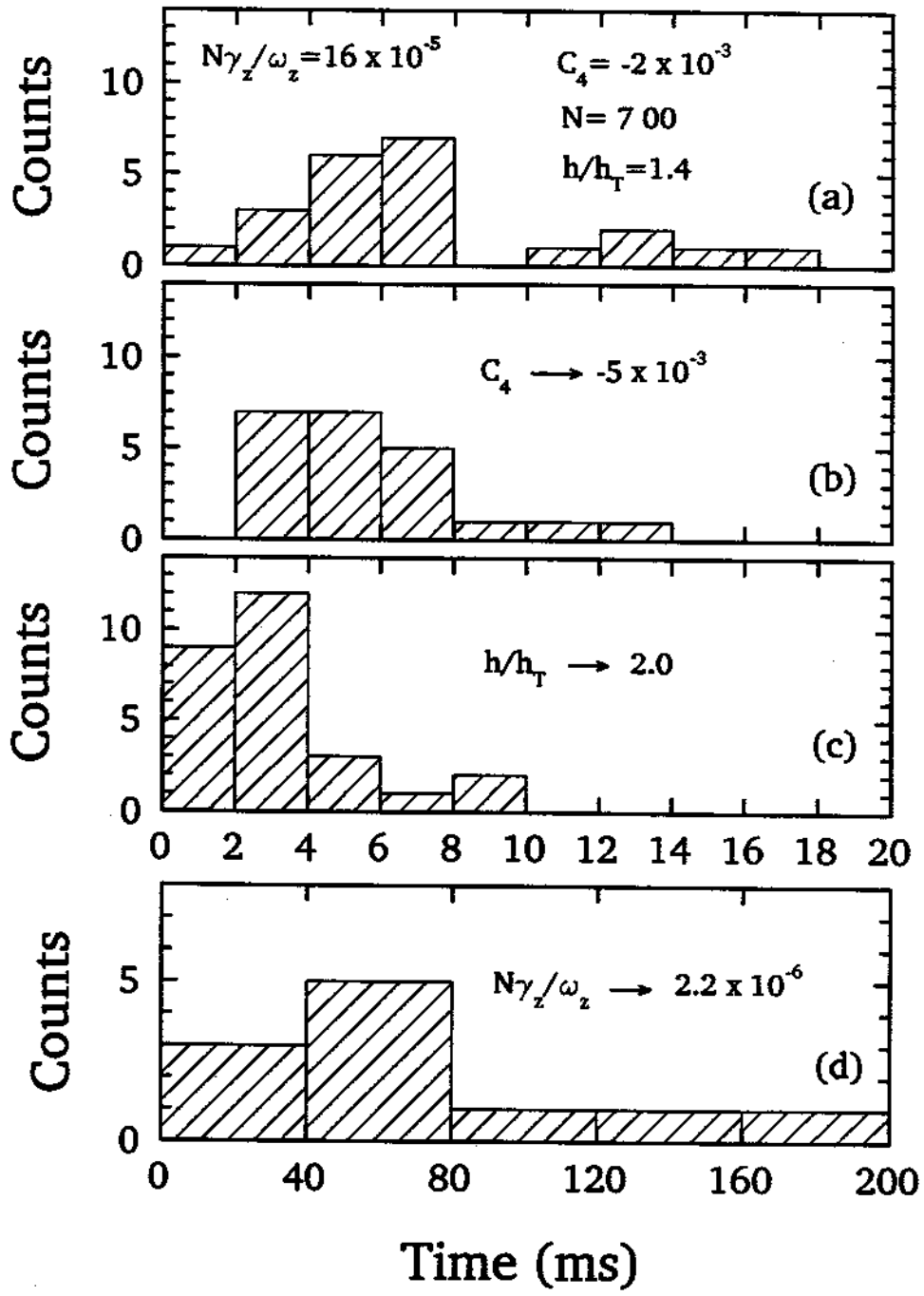

Figure 5.5: Distribution of jump times and variation with control parameters.

residence time is also observed to be longer for larger C_4 (Fig.5.6 b), presumably because a more anharmonic trap reduces internal energy. The internal energy may be lower since the amplitudes of de-synchronized oscillations would be smaller and the cooling via the LCR circuit is more efficient with larger anharmonicity. Phase switching rate increases rapidly with increasing internal energy. Consistent with this interpretation, an increase in the pump power or a stochastic modulation of the spring constant ω_z^2 (by applying a broadband noise potential to the ring) diminishes the mean residence time. The internal energy is conveniently controlled via the electron-cavity interactions. Fig. 5.6d shows the rapid decrease in mean residence time $\overline{\tau}$ for a cloud of $N = 400$ electrons as the frequency ω_c' is detuned from resonance with the TE_{115} cavity mode in Fig. 4.10. Transitions occur least frequently very near to resonance with a cavity mode (Fig. 5.2a) where the internal motion is most strongly cooled. The switching rate $\overline{\tau}^{-1}$ increases (Fig.5.2b) when a slight detuning of ω_c' from the mode resonance allows the internal energy to rise. As the decreasing residence times τ become comparable with the phase jump times τ_J, the CM motion can be expected to become "turbulent." Indeed, observed signals of the two phase-states are weaker and punctuated by random periods of incoherence. Further off resonance (cross-hatched region in Fig. 5.6d), the internal energy increases sufficiently so that the random, desynchronized motions of the electrons keep a detectable coherent CM motion from developing (Fig. 5.2c) because of the nonlinear couplings. Although a large anharmonicity can be introduced to increase cooling by the tuned circuit (presumably causing the dependence in Fig. 5.6b), we find that, in this "turbulent" region, long term coherent oscillation can not be restored by making the trap more anharmonic (increasing $|C_4|$).

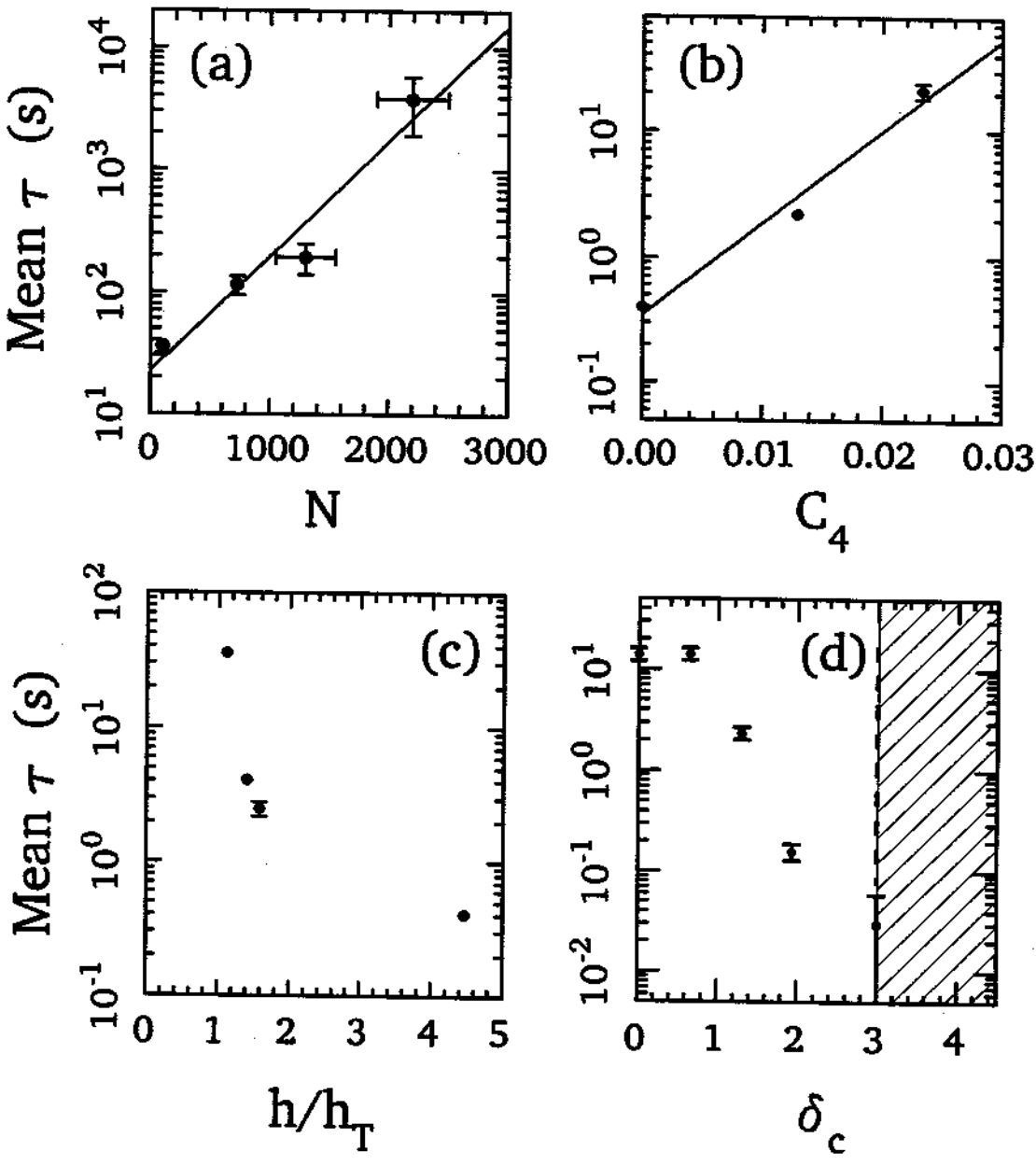

Figure 5.6: Dependences of mean residence time $\bar{\tau}$ on control parameters. Mean time between phase flips versus (a) number of electrons, (b) anharmonicity coefficient $|C_4|$, (c) pump strength h and (d) detuning between cyclotron frequency and a cavity mode eigenfrequency.

5.2 Partial Synchronization

The simplicity of the rigid model provides some understanding of the collective behavior in parametrically-pumped electron oscillators. But the model is inadequate in other important aspects. Parametrically-pumped electron oscillators are only partially synchronized. We now discuss observations of both the coherent and stochastic components of the CM motion, examining the frequency distribution of observed signal with a spectrum analyzer. The electron oscillators are pumped by a frequency synthesizer with very high spectral purity, suitable for high precision radio-frequency spectroscopy. We study changes in the spectrum brought about by varying a system parameter, such as the magnetic field (Fig. 5.8) to control

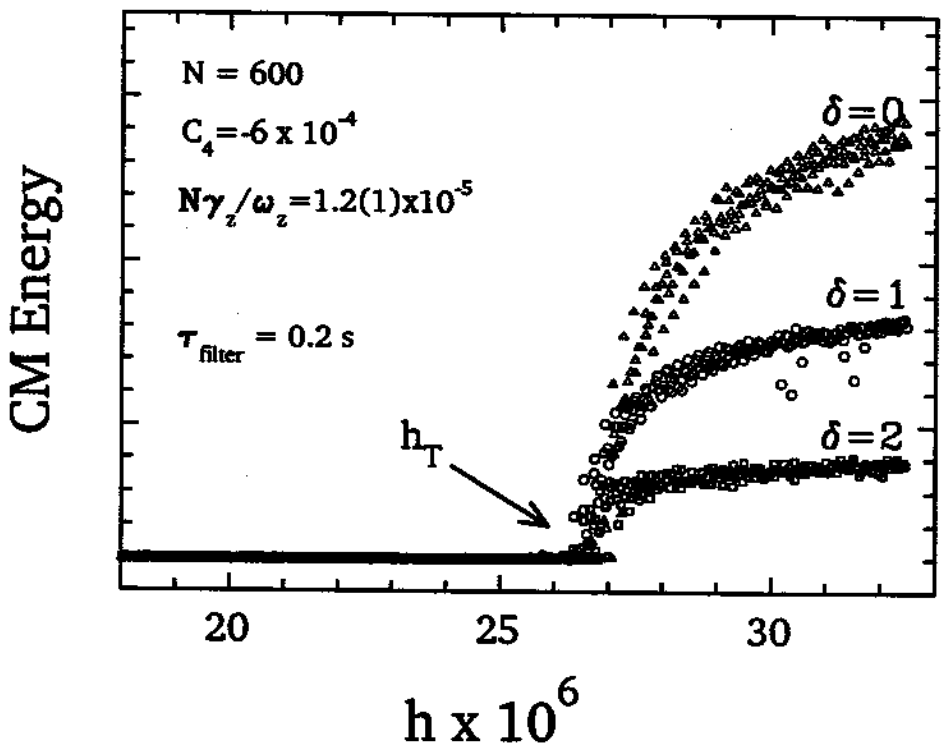

Figure 5.7: CM Energy versus pump strength for various detunings between cyclotron frequency and TE_{115} eigenfrequency. Saturation level is clearly limited by cyclotron cooling of internal motions.

radiative cooling of internal motions. The Fourier spectrum of the response above threshold consists of a broad "pedestal" due to fluctuations and a sharp peak which is orders of magnitude stronger due to the coherent motion. To have good signal for the the fluctuation spectrum, observed spectra are averaged over 100 samples. The highest three points in Fig. 5.8 (log-linear plot) shows the coherent component at $\nu_d/2$ decreasing as the internal energy is increased by detuning the ω_c from a cavity mode. Ignoring the coherent component, we observe that the spectrum of the fluctuations broadens with increasing detuning from a cavity mode (or internal energy).

The threshold of instability h_T is observed to be independent of internal energy, as illustrated in Fig. 5.7 (obtained by sweeping the pump strength for identical set of detunings used in Fig. 5.8), except for a small fluctuation at the 1% level. The energy in the coherent CM motion increases as the cyclotron frequency is tuned closer to the cavity eigenfrequency (for TE_{115}). It is noteworthy that Fig. 5.7 shows less noise in the measured mean squared amplitude for larger detunings from the cavity mode. It appears that the frequency spectrum broadens but amplitude noise is reduced when the cyclotron frequency is detuned from cavity mode resonance. A more detailed study of the amplitude and phase fluctuation as a function of cavity cooling would be interesting.

More evidence points to the limitations of the rigid model even when the radiative cooling of internal motions is maximized. With the electrons resonantly cooled by the mode TE_{115}, the Fourier spectrum is observed to change dramatically with increasing pump strength, as shown in Fig. 5.9 (Each spectrum is an average of 100 samples.). Only the broad, fluctuation spectrum is present below threshold (Fig. 5.9a). Observed width is of order $N\gamma_z/2\pi$ but becomes narrower as the pump strength approaches the threshold. When the pump strength exceeds h_T, a sharp peak (much narrower than the detection bandwidth of 5 Hz in Fig. 5.9a and 25 Hz in Fig. 5.9b) emerges from a larger pedestal. The pump strength is increased first in increments of +1 dB in Fig. 5.9 a, and then in increments

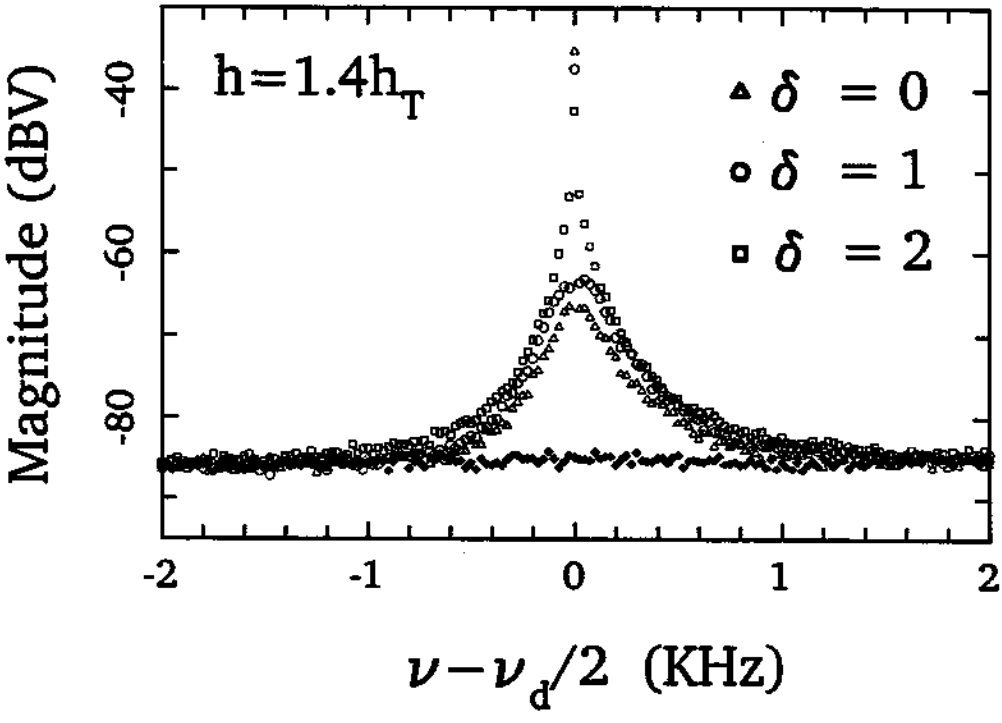

Figure 5.8: Fourier spectra of responses for various detunings from a cavity mode. Coherent response (peak) diminishes as cyclotron frequency is detuned from cavity mode eigenfrequency, but fluctuation spectrum broadens. Other system parameters are given in preceding figure.

of +2dB in Fig. 5.9 b. The fluctuation spectrum broadens as the pump strength increases and is skewed for high pump strengths (Fig. 5.9 b).

An important non-rigid feature with maximized cavity cooling is shown when the variation of signal size is plotted for a wide range of pump strengths. Fig. 5.10 plots the power in the peak (square) and the integrated power in the fluctuation spectrum (circle) versus pump strength for the data set shown in Fig. 5.9 . The integrated power of the fluctuation spectrum is the sum of contributions from each frequency bin with the white-noise background subtracted and the peak removed

by omitting the central bin. Above threshold, the coherent component grows with pump strength but saturates at $h \approx 1.6h_T$ and slowly decreases for $1.6h_T < h < 6h_T$. This is an important disagreement with the rigid model, which predicts the

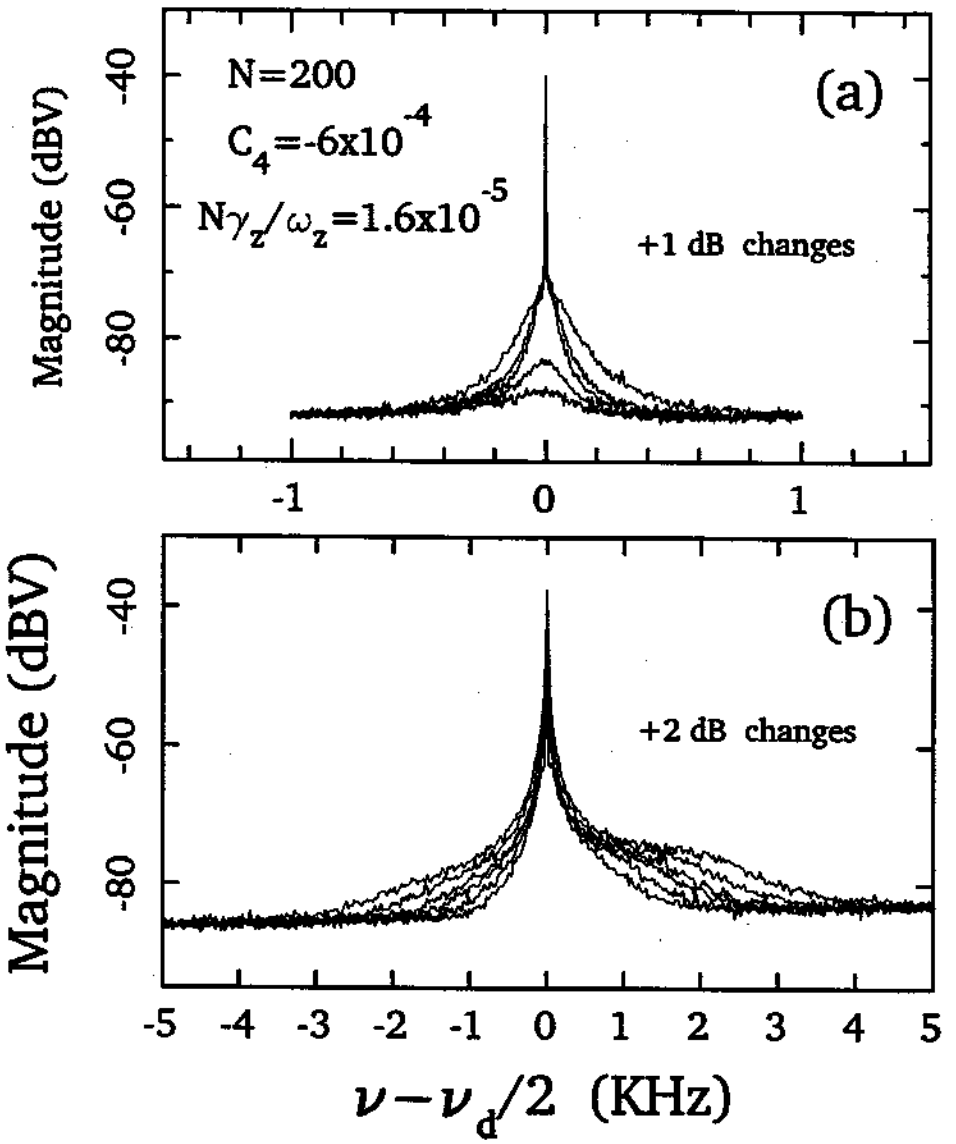

Figure 5.9: Fourier spectra for various pump strengths. A sharp peak emerges as pump strength exceeds threshold (a), with only broadband spectrum appearing below threshold. Fluctuation spectrum continues to broaden with increasing pump strength (b), becoming skewed for very strong pumping.

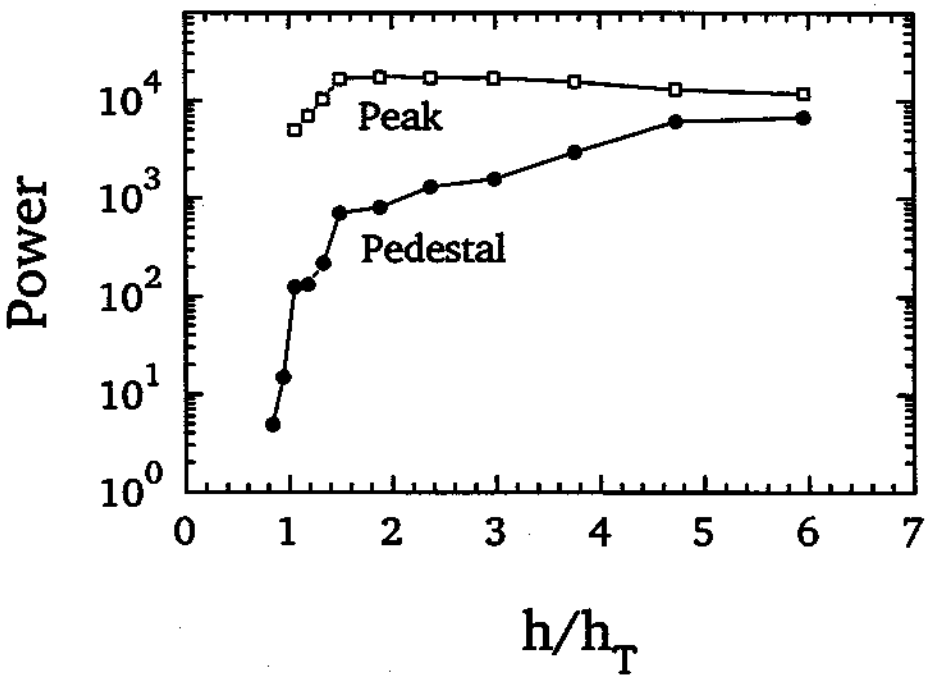

Figure 5.10: Comparison of power in the peak (square) with the integrated power in the fluctuation spectrum (circle) for the data set shown in preceding figure.

CM energy to be a monotonically increasing function of the drive strength (Sec. 3.3.1). For example, if the leading anharmonicity λ_4 is dominant, then the squared amplitude of the steady-state rigid motion goes as

$$A^2 \propto \sqrt{h^2 - h_T^2} \tag{5.4}$$

when drive frequency is $\omega_d = 2\tilde{\omega}_z$. On the other hand, Fig. 5.7 shows that observed energy in coherent CM motion is limited by cooling via radiation into the cavity, not by anharmonicity as would be the case for rigid motion. In spite of the disagreement, the observed lineshapes (Fig. 3.5) agree qualitatively with the rigid model (Fig. 3.4). Taking a linear lineshape like in Fig. 3.5a as an example, the lineshape is well preserved but the slope is observed to decrease when radiative cooling is reduced. The CM energy decreases also if the cyclotron oscillators are

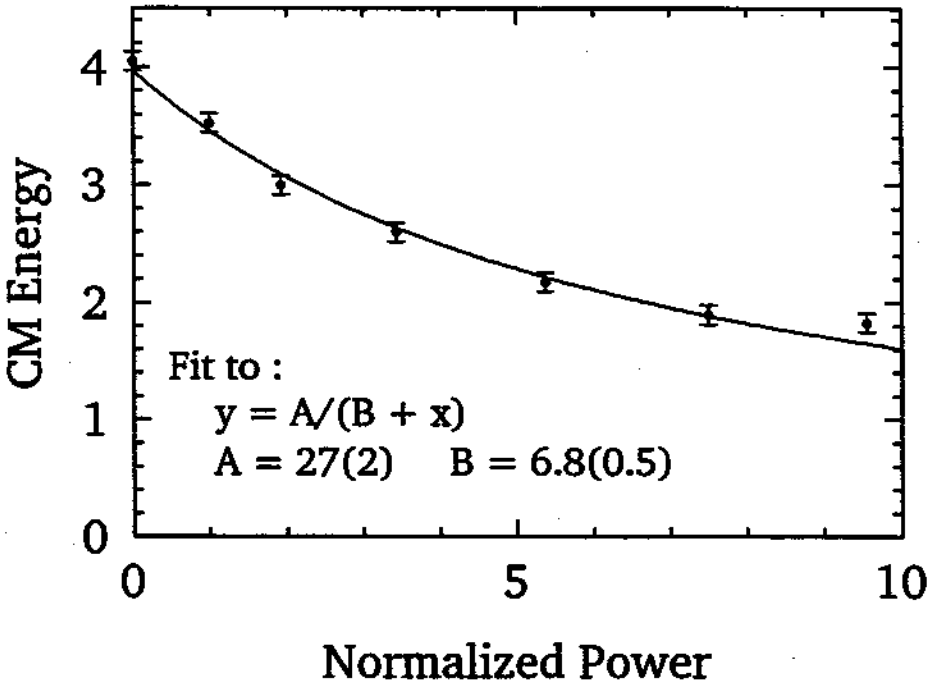

Figure 5.11: Decrease in coherent response to parametric excitation when cyclotron motions are heated with a microwave drive. Measured energy in axial CM energy with parametric drive at lower corner frequency $\nu_d = 2\nu_-$, is plotted versus normalized microwave drive power (dots). A simple form (solid) fits well to it.

heated up with a microwave drive, as illustrated in Fig. 5.11.

The mechanism causing the observed response to be so sensitive to both cyclotron cooling and anharmonicity is not understood. It appears that individual electron oscillators are excited to large amplitudes that are limited by anharmonicity, and that the observed coherent response is generated by their synchronized component which is controlled by a thermal process involving energy exchange between the axial and cyclotron motions. It is this sensitivity of partially synchronized motion to cooling of the internal motions (Fig. 5.7a) which has been very useful for probing the electron-cavity interactions (Fig. 4.1) so important for other radiative studies. We also find that the root-mean-squared (rms) saturation signal

scales linearly with the number of electrons (Fig. 5.12 a). The rms signal below threshold appears consistent with a linear dependence on the number of electrons, but the slope is about 50 times smaller (Fig. 5.12 b).

In contrast to the saturation and decline in power of the peak, we observe

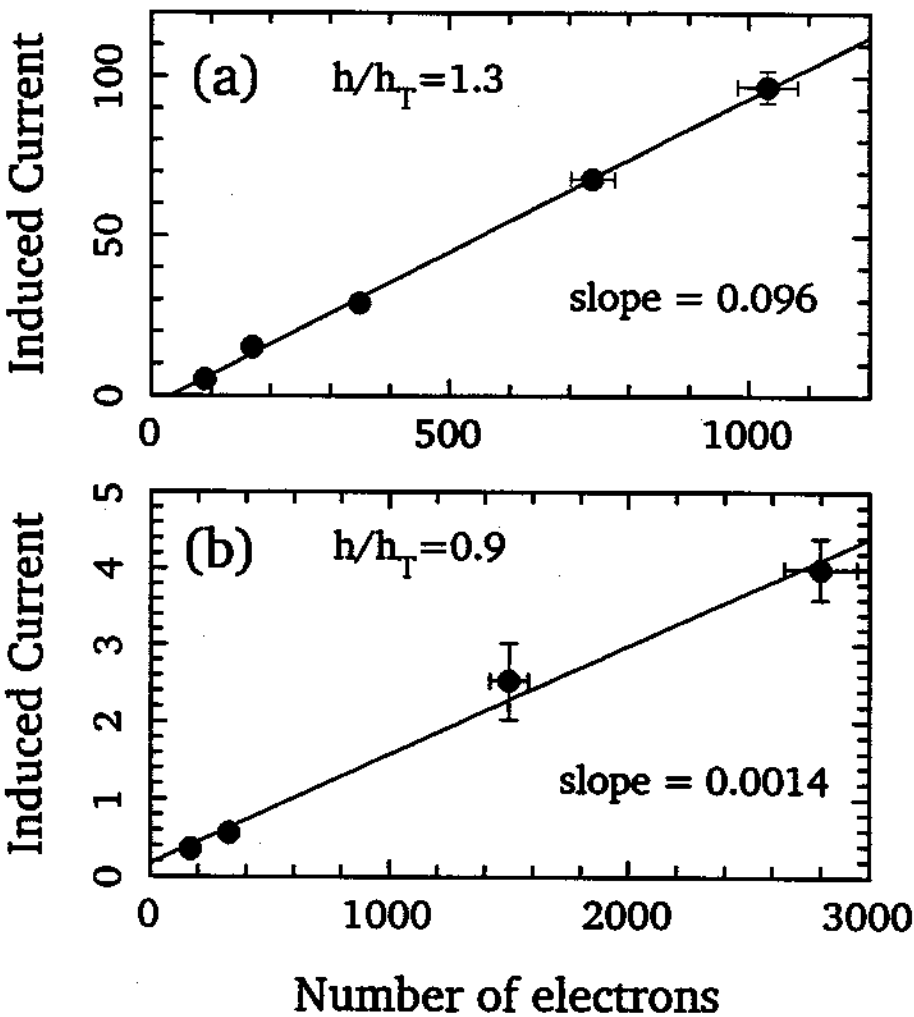

Figure 5.12: Scaling of rms induced current with number of electrons (a) above threshold and (b) below threshold.

that the power in the fluctuation spectrum increases monotonically for $h < 6h_T$ (Fig. 5.10) . The rate of growth in fluctuation power decreases with pump strength. There are a few step-like structures where the fluctuation spectrum changes very little with incremental rise in pump strength, but more data is needed to confirm this and to improve the resolution. The powers in the peak and pedestal are converging for $h < 6h_T$. It is not known if this convergence should continue for even higher pump strengths. Here again, the rigid model provides no clue.

5.3 Internal Motions: Slow Relaxations

A parametric drive excites not only the collective, CM motion of N electron oscillators but also internal degrees of freedom. Even for small systems (< 100 electrons), the full dynamics is difficult to analyze. In the past, a "bolometric" model [18,93] was developed for the disordered, thermal motions of trapped electrons or ions (summarized in Appendix B) and a simplified set of rate equations was thoroughly tested in experiments with electrons at $T \sim 80K$ [93]. In those early experiments, pulsed excitation showed that internal degrees of freedom come into thermal equilibrium so fast that they essentially form a single reservoir, with equilibration time shorter than other relaxation times. Since our apparatus is submerged in LHe, simplifying assumptions used in earlier studies may not apply at the lower temperatures. A few pulsed excitation experiments were carried out in our apparatus. For example, Fig. 5.13a shows the response when electrons initially at 4K are heated with a parametric drive below threshold in periodic 10-ms pulses. A storage oscilloscope captures the response from each pulse and gives an output averaged over 256 pulses to improve signal-to-noise. Fig. 5.13a shows the smooth relaxation which is characteristic of the response in a bolometric model [93] and, as expected, relaxation time is observed to be shorter when anharmonicity is increased ($|C_4|$ is made larger). This indicates that energy is transferred between internal reservoir and CM motion via the non-linear couplings. However, when the pump strength is above threshold, new features are observed. Fig. 5.13b

shows the substantially larger response of the partially coherent response to a single 250-ms pump pulse above threshold. This response has a rapid initial growth overshooting the steady state, characteristic of parametric resonance discussed in Chapter 3. Rapid growth stops abruptly and is followed by a much slower relaxation to a mean steady level with fluctuations. "Ring down" to the steady level (expected in rigid model, Fig. 3.2) is not observed, presumably because they are "washed out" by internal fluctuations. The slow relaxation to steady level is about 30 times longer than the typical rise time of the initial rapid growth, or observed relaxation times below threshold. Preliminary results from available data show that this new time constant is not very sensitive to changes in anharmonicity and pump strength. A more systematic study would extend over the full range of control parameters, including dependences on number of electrons and on detuning of cyclotron frequency from cavity mode resonance, etc.

To see that Fig. 5.13b is a difficulty for a bolometric model, we now give a simplified set of rate equations describing energy transfer between axial CM motion and internal reservoir. Another experimental evidence of its limitations follows. Below threshold, the bolometric model provides

$$C_z\dot{T}_z = -g_{zo}(T_z - T_o) + g_{iz}(T_i - T_z) + \dot{H}_z \tag{5.5}$$

$$C_i\dot{T}_i = -g_{io}(T_i - T_o) + g_{zi}(T_z - T_i) + \dot{H}_i \tag{5.6}$$

where, for simplicity, the tuned circuit and cavity are assumed to be at the same temperature T_o. The axial CM oscillator has temperature T_z with heat capacity C_z. A reservoir formed from all internal oscillations has temperature T_i with heat capacity C_i. Damping of the CM motion due to a tuned circuit is characterized by conductivity g_{zo}. Internal motions decay to T_o at a rate g_{io}/C_i. Energy transfer between CM motion and the internal reservoir is characterized by conductivity $g_{iz} = g_{zi}$. For sufficiently high temperatures, the thermal conductivities g_{ij} and heat capacities C_i are approximately independent of temperature. A set of linear, first-order differential equations, such as Eq. (5.5) and Eq. (5.6), cannot generate a response like in Fig. 5.13b.

Although this set of equations has been shown to be valid for temperatures above or near 80K for weak pumping of trapped electrons, [93] a more general system of equations would be necessary for electrons cooled to near LHe temper-

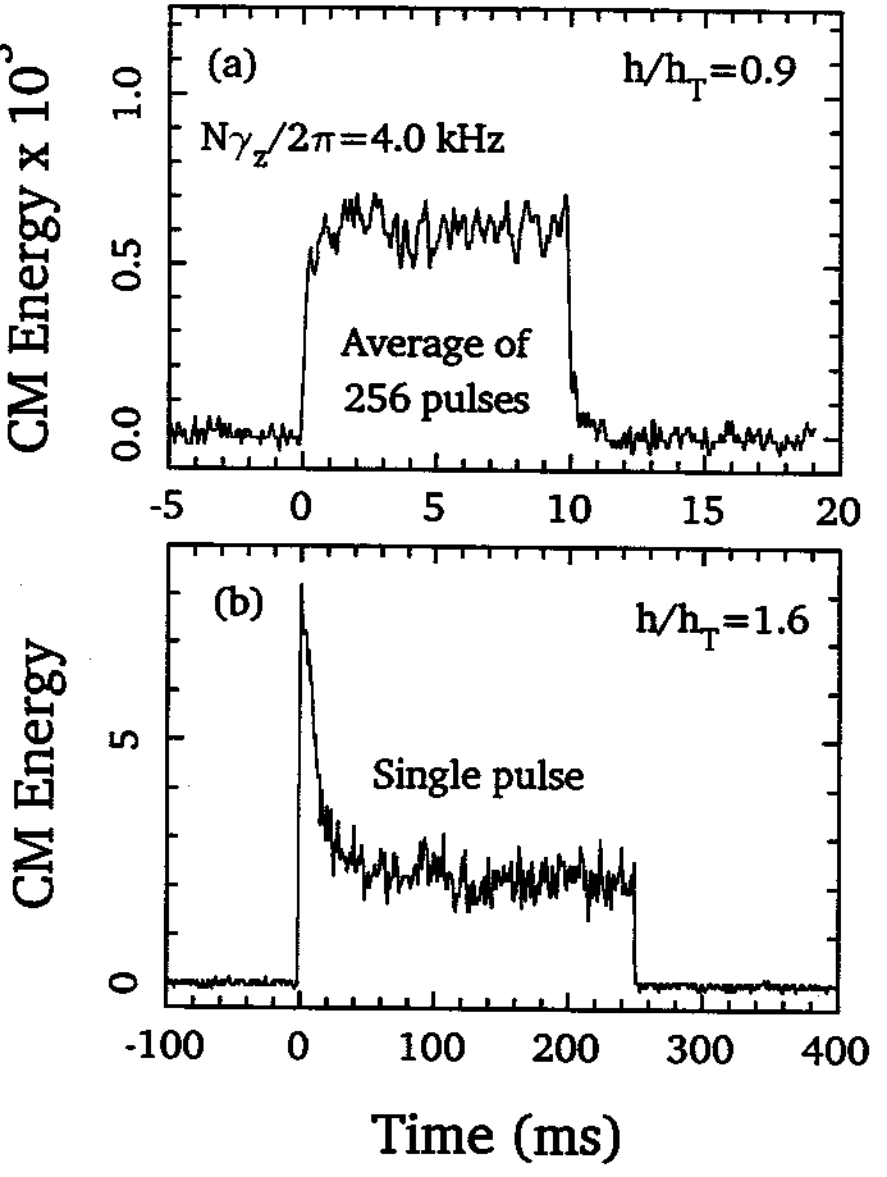

Figure 5.13: Characteristic responses to pulsed parametric pumping (a) below threshold and (b) above threshold. Averaging over 256 pulses improves the S/N below threshold (a), but only a single pulse is used above threshold (b). Slow relaxation (b) follows initial rapid growth, above threshold.

ature if the temperatures of the axial internal motions $T_{\|}$ and transverse internal motions $T_{\perp}$ do not equilibrate faster than other relaxation rates. Theoretical analysis of binary collisions in a strongly magnetized electron gas indicates a strong temperature dependence in this equilibration rate at very low temperatures, dropping rapidly as $T \longrightarrow 0$. [68] In our study, pulsed cyclotron excitations show some evidence for this. In Fig. 5.14, the energy in the axial CM motion of $N = 1600$ electrons is monitored with a storage scope as a square wave actives a microwave drive to excite the cyclotron motions for 10 s, and then deactivates the drive for the next 10 s. The output is averaged over many drive cycles. (Parametric drive is disconnected.) If the equilibration rate is significantly smaller at lower temperature, then the rise time in the energy of the axial CM motion when cyclotron heating

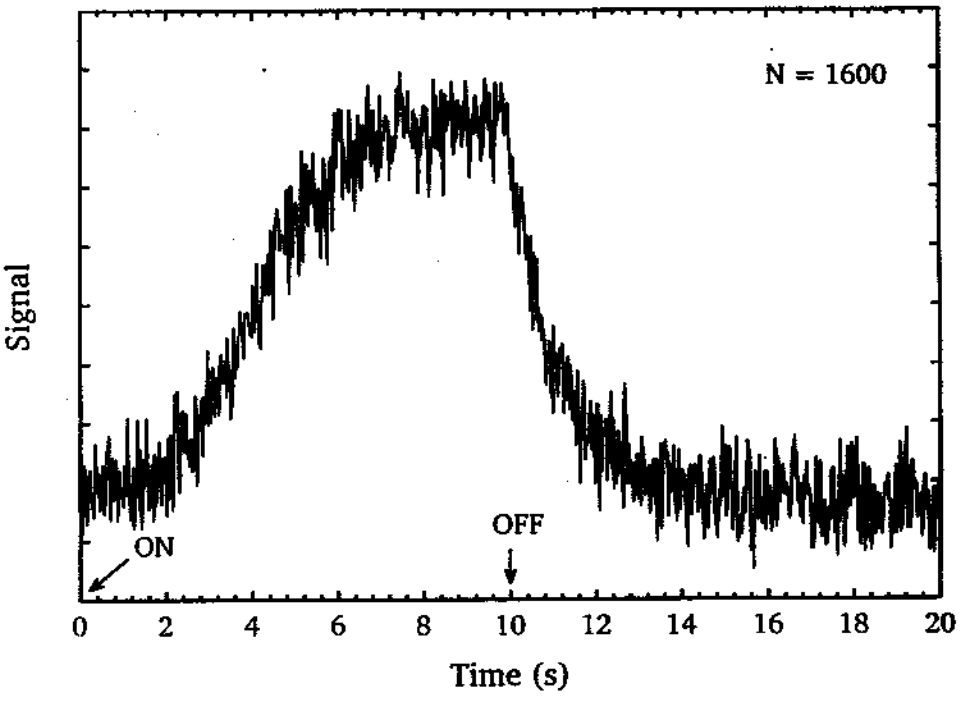

Figure 5.14: Pulsed cyclotron excitation. Slow growth and fast decay indicates temperature dependence of equilibration process.

is turned on would be much longer than the decay time when heating is turned off. Observed relaxation is clearly non-exponential with the rise time significantly longer than the decay time, indicating a slower relaxation at low temperatures. As shown in Fig. 5.14, nearly 2 seconds after the microwave drive was applied, observed axial CM energy increased by less than 10%, but faster growth followed. In contrast, axial CM energy has dropped by over 80% within 2 seconds after the drive was turned off. More detailed experimental study near 4K (at which 90% of cyclotron oscillators are in the ground state) may reveal other interesting features due to temperature dependent collisional processes and may establish a generalized set of rate equations for low temperatures.

5.4 Summary

A rigid model, in spite of its usefulness, does not provide a complete picture. A variety of interesting observations involve fluctuations due to internal motions, which are entirely omitted in a rigid model. Random transitions occur between the phase bistable states of partially synchronized CM motion. Except for very short times, observed residence times fit well to an exponential distribution (consistent with a two-level model with constant transition probability). Prompted by the "over-abundance" of rapid phase flips, observations on magnified time scales show interesting phase jump "trajectories," including a rare event showing synchronized CM motion oscillating in the basins of attraction for the two phase states. Measurements of mean time between flips are made for a wide range of conditions.

Partial synchronization is also examined in the Fourier transform of the observed response using a spectrum analyzer. A typical spectrum has a very sharp, narrow peak corresponding to synchronized motion, and a broadband, random distribution corresponding to fluctuations. As radiative cooling via coupling to a cavity standing wave is reduced, the sharp peak in the spectrum is reduced but the fluctuation "pedestal" is broadened. Even with radiative cooling maximized

(by tuning cyclotron motion into resonance with TE_{115}), the observed spectrum changes dramatically with pump strength. Power in the peak is observed to saturate as pump strength is increased above threshold and then decrease slowly for $h > 1.6h_T$, contradicting the monotonically increasing dependence expected of rigid motion. Only broadband, fluctuation spectrum is observed below threshold. The fluctuation pedestal broadens as the pump strength is increased above threshold, becoming skewed at high pump strengths. Integrated power in the pedestal grows monotonically with pump strength below $6h_T$, and may be converging to the same limit as the peak power.

Pulsed excitations give more evidence of limitations of a "bolometric" model developed for disordered, thermal motions below threshold. As expected, relaxation below threshold is observed to depend on anharmonicity, indicating energy exchange between center-of-mass and internal motions. Above threshold, however, response to pulsed excitation is characterized by a rapid growth which is abruptly stopped and followed by slow relaxation to a lower, mean coherent oscillation with fluctuations. Furthermore, for our apparatus at $\sim 4K$, pulsed cyclotron excitation (with parametric drive switched off) indicates strong temperature dependence in equilibration process for internal motions, requiring a more complicated, generalized model at low temperatures.

These interesting observations in parametrically-pumped electron oscillators demonstrate the fine control over a wide range of system parameters which is available for precise, quantitative studies of fluctuation phenomena. A more detailed theoretical treatment of this system, hopefully, will give a better understanding of the observations and measurements presented, which may lead to new experiments.